

Article

Towing Performance of the Submerged Floating Offshore Wind Turbine under Different Wave Conditions

Conghuan Le ¹ , Jianyu Ren ¹, Kai Wang ^{2,*} , Puyang Zhang ¹  and Hongyan Ding ¹

¹ State Key Laboratory of Hydraulic Engineering Simulation and Safety, Tianjin University, Tianjin 300350, China; leconghuan@163.com (C.L.); jianyu_ren@163.com (J.R.); zpy_td@163.com (P.Z.); dhy_td@163.com (H.D.)

² School of Marine Engineering and Technology, Sun Yat-sen University, Zhuhai 519082, China

* Correspondence: wangkai25@mail.sysu.edu.cn

Abstract: One of the advantages of floating offshore wind turbines (FOWTs) is that they can be designed to be easily wet towed and installed to reduce the cost of offshore construction. In this paper, a fully coupled towing system numerical model is established for a novel 10 MW FOWT concept, namely, a submerged floating offshore wind turbine (SFOWT) to investigate the towing performance. Firstly, the numerical simulation is validated by comparison with model experiment results. Then, a series of numerical simulations are conducted to predict and compare the towing performance for a three-column SFOWT (TC-SFOWT) and a four-column SFOWT (FC-SFOWT) under different wave conditions. The results show that the two forms of SFOWT have good towing performance when the significant wave height is less than 5 m, which is the maximum wave height for the allowable towing condition. The FC-SFOWT shows relatively better performance in heave motion and roll motion, but the towing force is relatively larger compared with the TC-SFOWT under the same condition. When the significant wave height is 5 m, the maximum values of heave motion, pitch motion, and roll motion of the TC-SFOWT are 2.51 m, 2.14°, and 1.38°, respectively, while they are 2.25 m, 2.70°, and 1.21°, respectively, for the FC-SFOWT. Both the roll motion and the pitch motion are satisfied with the requirement that the roll and pitch are less than 5° during the towing process. The mean towing force of FC-SFOWT is 159.1 t at the significant wave height of 5 m, which is 52.8% larger than that of TC-SFOWT. The peak period mainly influences the frequency where the response peak appears in power spectra. The findings in this paper could provide some guidelines for wet towed operations.

Keywords: submerged floating offshore wind turbine; integrated towing; wave period; wave height



Citation: Le, C.; Ren, J.; Wang, K.; Zhang, P.; Ding, H. Towing Performance of the Submerged Floating Offshore Wind Turbine under Different Wave Conditions. *J. Mar. Sci. Eng.* **2021**, *9*, 633. <https://doi.org/10.3390/jmse9060633>

Academic Editor: Yingyi Liu

Received: 15 May 2021

Accepted: 2 June 2021

Published: 6 June 2021

Publisher's Note: MDPI stays neutral with regard to jurisdictional claims in published maps and institutional affiliations.



Copyright: © 2021 by the authors. Licensee MDPI, Basel, Switzerland. This article is an open access article distributed under the terms and conditions of the Creative Commons Attribution (CC BY) license (<https://creativecommons.org/licenses/by/4.0/>).

1. Introduction

The wind resource has the advantages of higher wind speed, stable propagation direction, lower turbulence intensity, and free surface roughness in the far-reaching sea. With the exhaustion of the shallow wind power resource, it is of great interest to explore offshore wind power in deeper and farther ocean areas. Due to the dramatically increased costs and limitations with regards to the maximum operational depth of wind turbine installation vessels, the traditional fixed foundation may no longer be feasible for sea areas with a water depth greater than 60 m. The floating offshore wind turbine (FOWT) seems to be a feasible solution for the development of wind power in the deep sea. In 2017, Hywind Scotland, the world's first commercial floating wind power project, was officially put into operation in Scotland [1]. By the end of 2020, the wind power generation of FOWTs around the world has reached 125 MW [2]. In recent years, engineering and academia around the world have put forward various forms of foundations for FOWTs [3–6]. The FOWTs have many advantages; for example, they are not limited by water depth and geological conditions, are easy to dismantle, have little impact on the environment, and are suitable for

high-power wind turbines [7]. On the other hand, they can be wet towed to the installation sites through self-floating, which is another significant advantage of the FOWTs.

For the wet towing performance of marine structures, scholars have carried out a few research works mainly focused on the stability of the towing system and towing resistance. Strandhagen et al. [8] studied the towing system based on linear theory and found that changing the frequency of the towing point and the length of towing line can make the towing system have better stability. Inoue et al. [9–11] used the linear theory to study the course stability of the towing system under multiple tugboats and found that the elasticity of the towing line and the weight of the object being towed have great influence on the course stability of the towing system. Varyani et al. [12] carried out numerical simulation on the towing operation of damaged ships and pointed out that wind load is the main factor affecting the stability of the towing system.

FOWTs have a high center of gravity and are subjected to the complicated environmental loads such as wind, waves, and currents in addition to the towing force during the transport phase. Thus, how to ensure the safety of transportation for FOWTs is one of the urgent problems to be addressed. In recent years, scholars have carried out preliminary research on the towing operation process for FOWTs with different types of foundation. Collu et al. [13] studied the static stability criterion of the towing process of FOWTs under a normal and severe environment and provided the calculation guidelines for the maximum values of the metacentric height and the maximum height of the towing lines, and then applied the results to design the semi-submersible floating foundation for NOVA FOWT to evidence the overall good performance of those rules. Myland et al. [14] conducted an experiment to study the towing stability of the GICON[®]-TLP under two different carriage speeds in the calm water and two different regular wave conditions. Two different configurations, including a squared configuration and a diagonal configuration of the GICON[®]-TLP, were performed to determine which configuration had a lower resistance and a better seakeeping performance. The results showed that the towing speed and wave height had significant influence on the stability and towing resistance and the diagonal configuration had a lower resistance than the squared configuration because the truss structure of the squared configuration had no hydrodynamic permeability. Moreover, the non-stationary flow, which causes detachment at the cylindrical buoyancy bodies, would generate an oscillating sway motion. Ding [15–18] designed a submerged floating foundation for supporting an NREL5 MW wind turbine, and conducted a lot of research on the dynamic response of the SFOWT in complex environmental conditions. Han et al. [19] put forward a towing system model of the SFOWT based on multi-body dynamics theory to study the wind, waves, currents, and height of the towing point on motion response of the SFOWT during the towing phase. The results show that under the standard environmental conditions, the inclination of the SFOWT meets the requirements of the standard [20] that the absolute acceleration of heave is less than 0.2 g, but the viscous damping of the SFOWT does not get considered in the towing analysis.

It is critical to be able to predict reliably the towing behavior of the FOWT in the real sea environment. In this paper, two forms of SFOWT, namely TC-SFOWT and FC-SFOWT, with the similar mass and same center of gravity, are designed to support the DTU-10MW reference wind turbine [21] in Section 2, as shown in Figure 1. The theory background is presented in Section 3. The validation of the numerical model is firstly verified by model experiments in Section 4. The towing performance of the two forms of SFOWTs under different wave conditions during the towing process are discussed by frequency domain and time domain analysis in Section 5. The conclusions are summarized in Section 6.

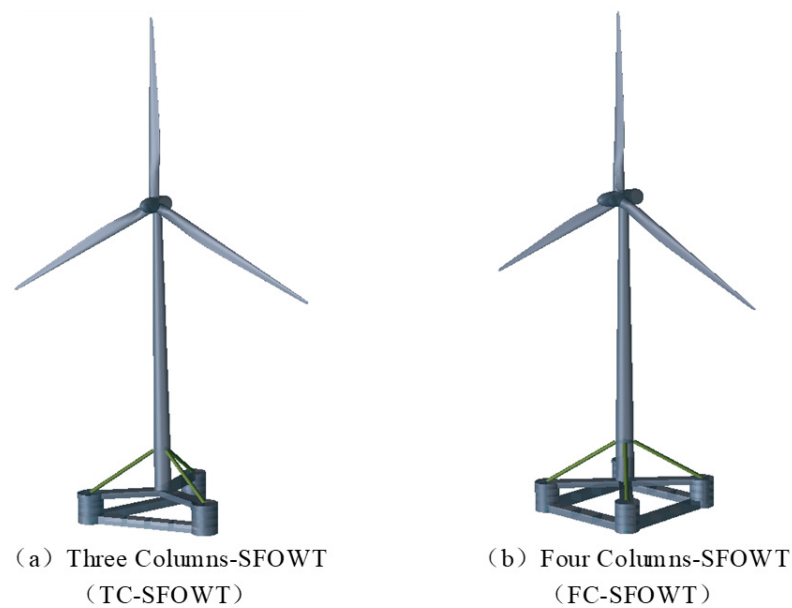


Figure 1. Overall model of SFOWTs.

2. SFOWTs and Integrated Towing System

An SFOWT is composed of a DTU 10MW reference wind turbine [21], which was released by the Danish University of Technology (DTU) and has been widely accepted by academia, and a submerged floating foundation. The main parameters of the DTU 10MW reference wind turbine are given in Table 1, and the main parameters of the towing system of SFOWTs are presented in Table 2. The submerged floating foundation is composed of a center column, three or four columns connected by horizontal pontoons, and three or four cross braces and diagonal braces. The side columns and horizontal pontoons provide the buoyancy for SFOWTs during the towing process [16]. The wind turbine tower is installed at the top of the center column, as shown in Figure 2. Because of the relatively large water plane area and shallow draft, the SFOWTs are semi-submersible and self-stabilized during the towing process.

Table 1. Main parameters of the DTU 10MW reference wind turbine [21].

Item	Value
Rated power (MW)	10
Cut-in, rated, cut-out wind speeds (m/s)	4, 11.4, 25
Number of blades	3
Diameter of rotor (m)	178.3
Blade length (m)	86.366
Hub height (m)	119
Mass of impeller, nacelle, tower (kg)	227,962, 446,036, 628,422
Overall center of gravity (CoG) (m)	(−0.3, 0.0, 85.5)

The numerical simulation of the SFOWT towing system were carried out in the time domain based on the Sesam software developed by DNV GL. First, as shown in Figure 1, the panel models and mass models of the two forms of SFOWT were established according to the parameters listed in Tables 1 and 2 in the GeniE module [22]. Then, the panel model and mass model were imported into the HydroD module [23], frequency domain analysis was performed using the Wadam code based on potential flow theory and considering the viscous damping (see Section 5.2), and the hydrodynamic coefficients such as the added mass, radiation damping, hydrostatic restoring stiffness, and transfer functions of the SFOWT were obtained in the frequency domain. Additionally, these hydrodynamic coefficients were then fed to the SIMO module [24]. In the SIMO module, a towing line

was set up with a length of 100 m and bridle angle of 60°. A constant bollard pull force was applied to maintain a towing speed of 4 knots. The dynamic responses of the towing system of the FC-SFOWT and TC-SFOWT were predicted in the time domain based on the potential flow theory in the SIMO module. Each simulation lasted three hours with the time step of 0.2 s, in which the first 1000 s were removed to eliminate the transient effect. The bird’s eye view of the towing system in SIMO is shown in Figure 3. The wave direction during the towing process was 180°, as shown in Figure 4.

Table 2. Main parameters of the towing system of SFOWTs.

Item	TC-SFOWT	FC-SFOWT
Diameter of center column (m)	8.3	8.3
Diameter of vertical pontoon (m)	12.68	11.0
Diameter of side column (m)	15.0	15.0
Distance between side column (m)	61.24	50.0
Width and height of horizontal pontoon (m)	6.3, 4.4	6.6, 4.0
Diameter of diagonal brace (m)	2.5	2.5
Towing speed (knots)	4	4
Draft (m)	5.2	6.0
Angle of towing bridle (°)	60	60
Length of towing line (m)	100	100
Mass of platform (kg)	4,819,000	4,812,000
Mass moment of inertia in roll (kg·m ²)	1.94×10^9	2.31×10^9
Mass moment of inertia in pitch (kg·m ²)	1.94×10^9	2.31×10^9
Mass moment of inertia in yaw (kg·m ²)	3.41×10^9	4.02×10^9

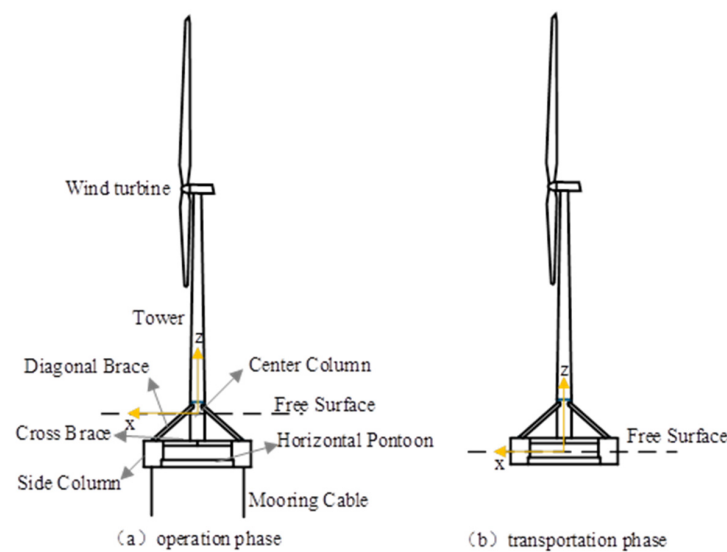


Figure 2. The structure of the SFOWT.

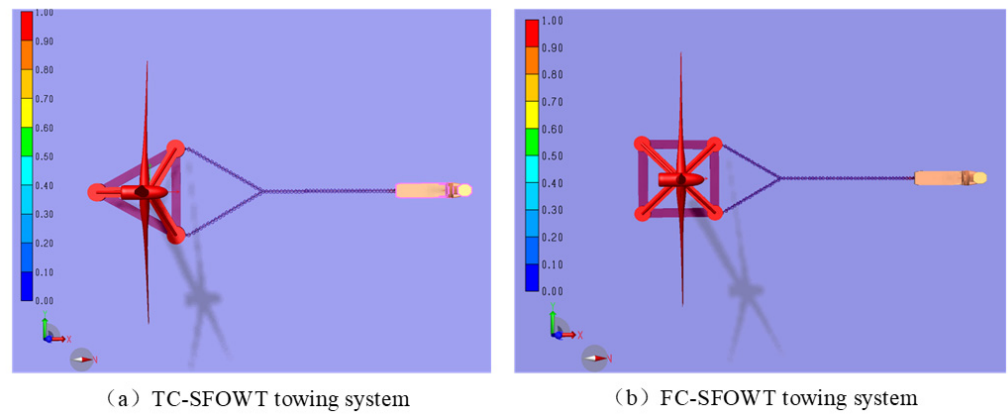


Figure 3. Bird's eye view of the TC-SFOWT and FC-SFOWT towing system.

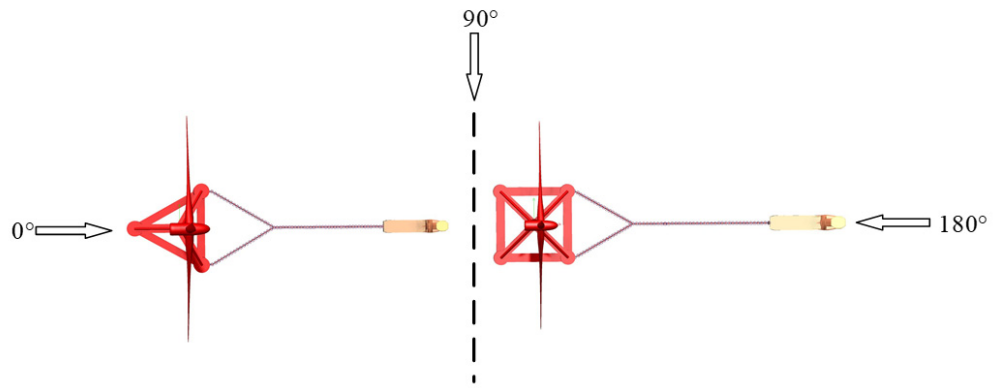


Figure 4. Definition of wave directions under the towing condition.

3. Theory

3.1. Hydrodynamic Load

The hydrodynamic coefficients are calculated using the Wadam code based on the potential flow theory, which mainly includes radiation force, diffraction force, and hydrostatic pressure [25].

$$F_i^{Hydro} = F_i^{Waves} + \rho g V_0 - C_{ij}^{Hydrostatic} q_j - \int_0^t K_{ij}(t - \tau) \dot{q}_j(\tau) d\tau - A_{ij} \ddot{q}_j \quad (1)$$

where F_i^{Waves} is the diffraction wave force, $\rho g V_0 - C_{ij}^{Hydrostatic} q_j$ is hydrostatic pressure, $\rho g V_0$ is static buoyancy, ρ is the density of water, g is the acceleration of gravity, and V_0 is drainage volume of platform. $C_{ij}^{Hydrostatic} q_j$ is the hydrostatic restoring force and $C_{ij}^{Hydrostatic}$ is the restoring stiffness matrix. $-\int_0^t K_{ij}(t - \tau) \dot{q}_j(\tau) d\tau - A_{ij} \ddot{q}_j$ is the radiation wave force, where K_{ij} is a delay function and τ is a dummy variable, and t is the simulation time, A_{ij} is the added mass, $q_j(t)$ and $\dot{q}_j(\tau)$ represent the displacement and velocity of the SFOWTs in the j th degree of freedom.

The wave directions when calculating hydrodynamic parameters are shown in Figure 5.

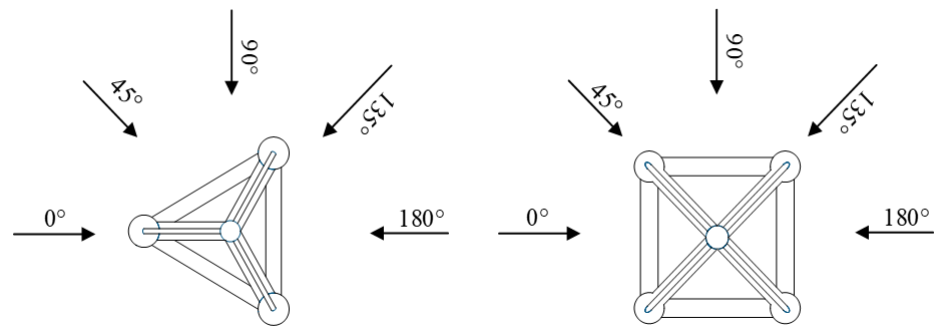


Figure 5. Wave directions.

3.2. Equation of Motion of Towing System

The equation of motion of SFOWTs in waves can be expressed as follows [26].

$$F_{Ti} = \sum_{j=1}^6 M_{ij} \ddot{x}_j \tag{2}$$

where F_{Ti} is the total external force on the i th degree of freedom, M_{ij} is the mass inertia force coefficient of the SFOWTs, \ddot{x}_j is the acceleration in surge, sway, heave, roll, pitch, and yaw motion of the SFOWTs, $j = 1, 2, 3, 4, 5, 6$.

$$F_{Ti}(t) = F_i^{Hydro}(t) + F_i^{towing}(t) + F_i^{vis}(t) \tag{3}$$

where $F_i^{Hydro}(t)$ is hydrodynamic force, $F_i^{vis}(t)$ is the viscous force, and $F_i^{towing}(t)$ is the towing force.

$$\{M_{ij}\} = \begin{Bmatrix} m_0 & 0 & 0 & 0 & m_0 z_G & 0 \\ 0 & m_0 & 0 & -m_0 z_G & 0 & 0 \\ 0 & 0 & m_0 & 0 & 0 & 0 \\ 0 & -m_0 z_G & 0 & I_{11} & 0 & 0 \\ m_0 z_G & 0 & 0 & 0 & I_{22} & 0 \\ 0 & 0 & 0 & 0 & 0 & I_{33} \end{Bmatrix}$$

where m_0 is the mass of SFOWTs, z_G is the vertical coordinate of the center of gravity for SFOWTs, and I_{ii} is the mass moment of inertia of SFOWTs, $i = 1, 2, 3$.

4. Model Validation

To validate the numerical model, a series of experiments were carried out at a Froude scale of 1:80. Figures 6 and 7 show the schematic diagram of the experiment and the model-scale of the 10 MW TC-SFOWT and FC-SFOWT, respectively. One environmental condition was used for the comparisons, as shown in Table 3. The pitch motion and the towing force obtained by numerical simulation and experiments are shown in Table 4. The comparison results show good agreement between the numerical predications and the experiment results, which means the numerical simulation can predicate the towing responses with high accuracy.

Table 3. Load case for verification of numerical model.

Significant Wave Height (m)		Peak Period (s)		Towing Speed (m/s)	
Simulation	Experiment	Simulation	Experiment	Simulation	Experiment
5	0.0625	8.9	1.0	2.06	0.23

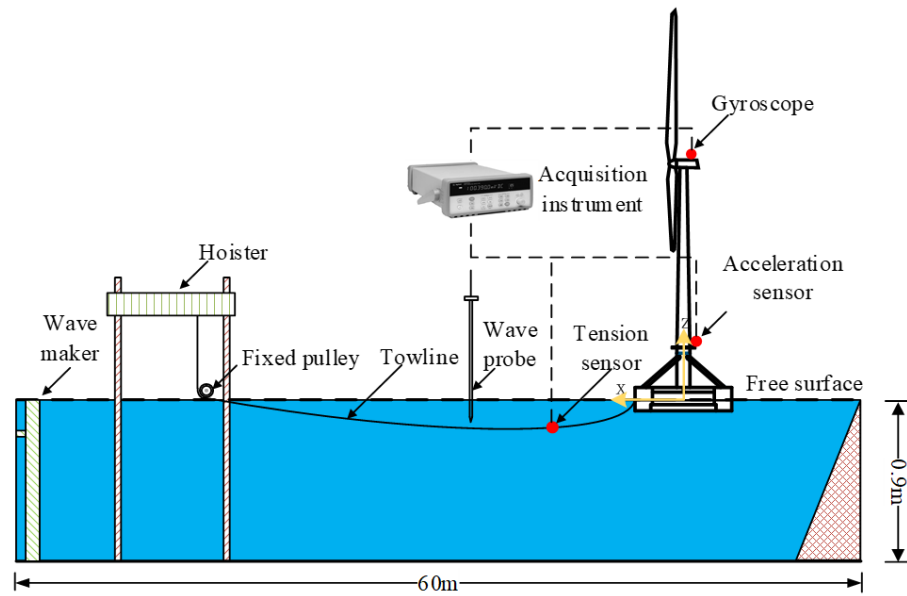


Figure 6. Schematic diagram of towing experiments.



(a)



(b)

Figure 7. Model-scale of 10MW TC-SFOWT and FC-SFOWT in the wave basin. (a) TC-SFOWT, (b) FC-SFOWT.

Table 4. Comparison results for model validation in full scale. (Note: Num., Exp., and Max. are the abbreviations for numerical, experimental, and maximum).

Pitch Motion (°)				Towing Force (N)			
TC-SFOWT		FC-SFOWT		TC-SFOWT		FC-SFOWT	
Num. Max.	Exp. Max.	Num. Max.	Exp. Max.	Num. Mean	Exp. Mean	Num. Mean	Exp. Mean
2.446	2.746	2.704	2.587	1,200,543	1,254,400	1,771,500	1,690,562

5. Results and Discussion

5.1. Wave Motion Transfer Functions (RAOs)

The RAOs in the heave, roll, and pitch motion were analyzed, as shown in Figures 8–10. It can be seen from Figure 8 that the heave motion RAOs were less affected by the wave direction, and when the period of incident wave was less than 32 s, the heave motion RAOs of two forms of SFOWT were greatly affected by the wave period. TC-SFOWT has two extremums around 6 and 12 s, and FC-SFOWT has three extremums around 5, 10, and 15 s for heave RAOs. When the wave period was greater than 32 s, the heave motions were less affected by the wave period and tend to be stable at maximum of the two forms of SFOWT.

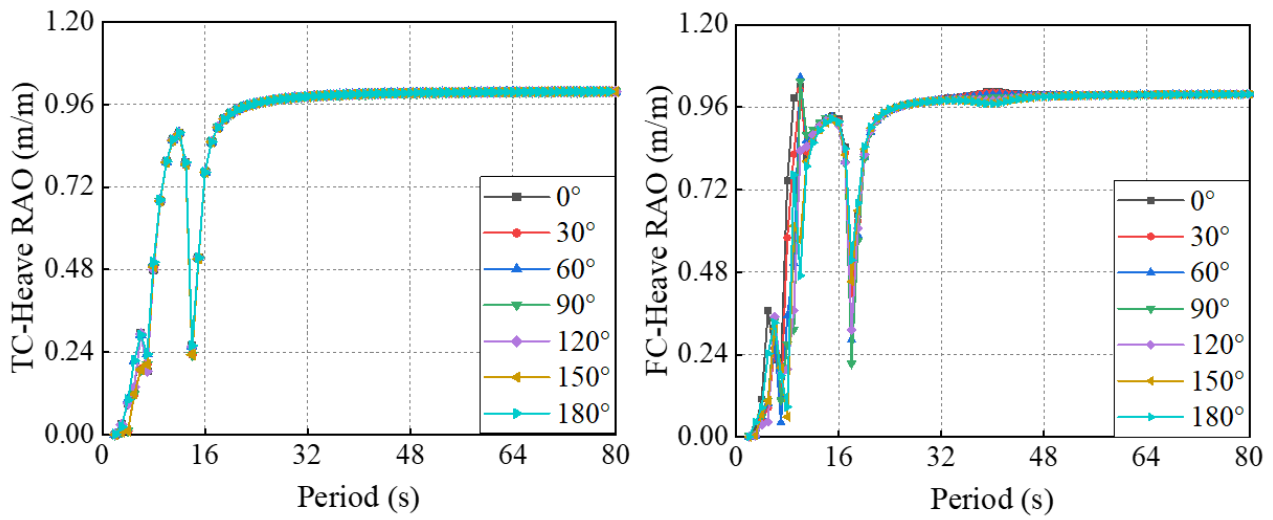


Figure 8. Heave motion RAOs of SFOWTs.

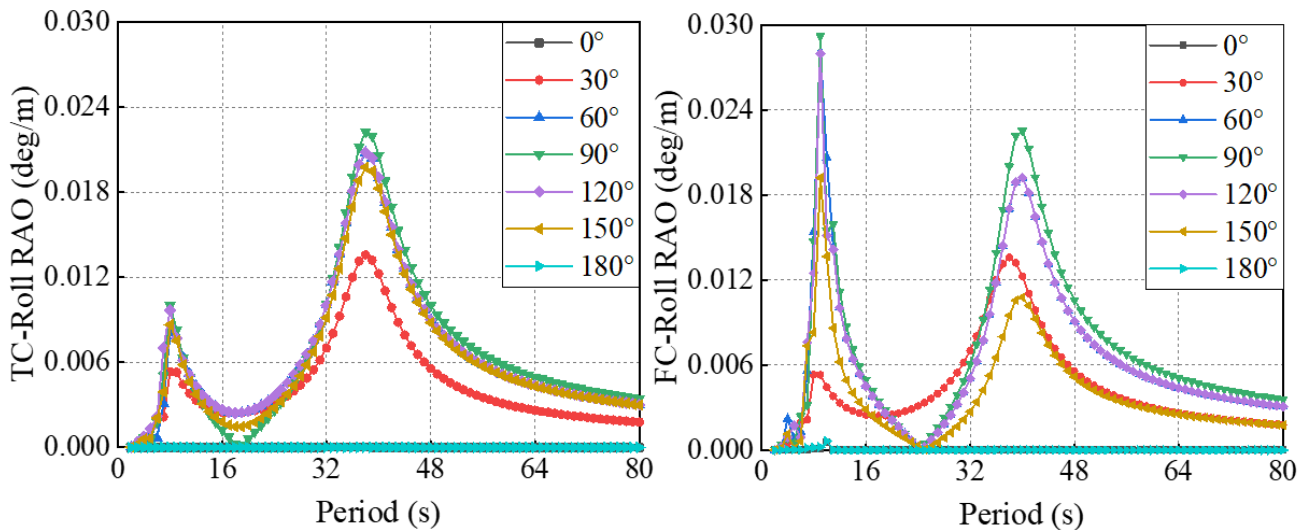


Figure 9. Roll motion RAOs of SFOWTs.

The wave directions had a great influence on the roll motion RAOs of the two forms of SFOWT as shown in Figure 9. With the increase of the wave period, the roll motion RAOs show a trend of increase first, and then decrease. TC-SFOWTs have two extremums around 9 and 38 s, which are 0.0097 and 0.022° / m, respectively, and FC-SFOWTs have two extremums also around 9 and 40 s, which are 0.029 and 0.022° / m, respectively. The extremums of roll motion RAOs for the two forms of SFOWT appear at the wave direction of 90° and tend to 0° / m when the wave directions were 0 and 180°. The roll RAOs of the

two forms of SFOWT were similar in long-period wave conditions, but the short-period wave had great influence on the roll motion RAOs of the FC-SFOWT.

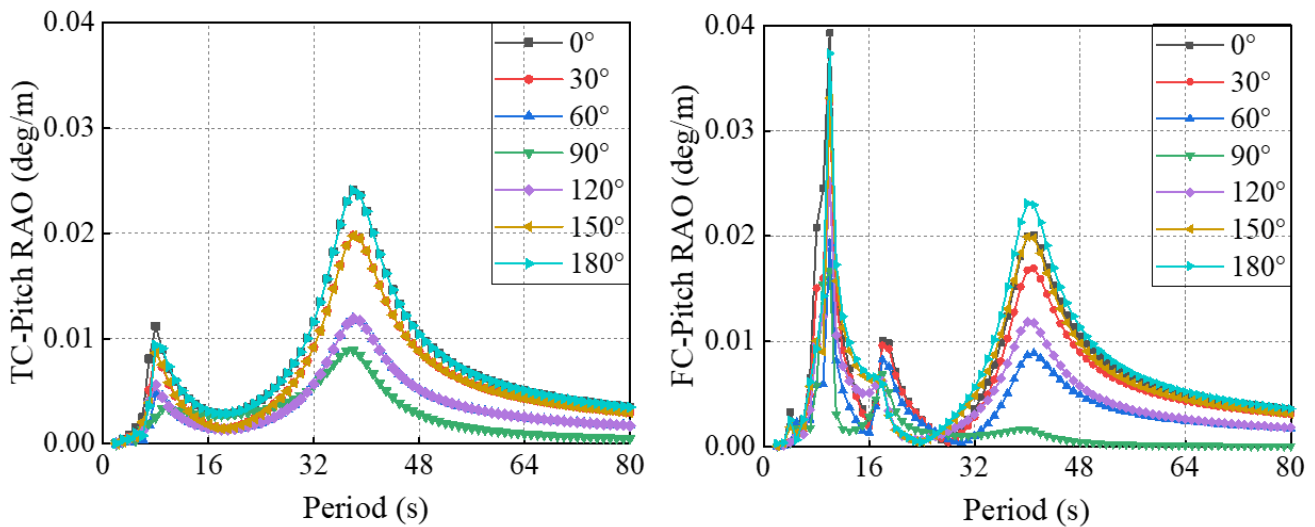


Figure 10. Pitch RAOs of SFOWTs.

As depicted in Figure 10, the pitch motion RAOs of SFOWTs were also greatly affected by the wave direction. TC-SFOWTs have two extremums around 8 and 38 s, which are 0.011 and 0.024° /m, respectively, and FC-SFOWTs have three extremums around 10, 18, and 40 s, which are 0.039, 0.010, and 0.023° /m for pitch motion RAOs, respectively. The extremums all appear at the wave directions of 0 and 180°. The pitch motion RAOs were greatly influenced by short-period waves for FC-SFOWTs, and the changes of RAOs in the pitch and roll motions of the two forms of SFOWT are similar.

5.2. Viscous Damping

The RAOs of SFOWTs were calculated based on the potential flow theory, and therefore, only the potential damping of the SFOWTs was considered and the viscous damping was ignored, which leads to a larger calculation result than the actual value of RAOs in six DOFs (degree of freedoms). In order to make the calculation results subsequently more accurate, this paper calculated the viscous damping of SFOWTs to correct the calculation process. In this paper, the method in reference [27] was adopted, and 10% of the critical damping was taken into account. The inertial mass, added mass, and restoring stiffness of the structure were derived from the calculation results of hydrodynamic parameters, and the viscous damping of SFOWTs was calculated by—Equation (4). The results are summarized in Table 5.

$$\beta_0 = 2\sqrt{(M + M_a) \times C_i} \tag{4}$$

where β_0 is critical damping, M is mass matrix of the SFOWTs, M_a is added mass matrix, and C_i is restoring stiffness matrix.

Table 5. Viscous damping for SFOWTs.

DOFs		Inertial Mass (kg)	Added Mass (kg)	Restoring Stiffness (N/m, N/rad)	Viscous Damping (N/(m/s), N(rad/s))
Heave	TC-SFOWT	6.02×10^6	6.94×10^6	3.78×10^6	1.40×10^6
	FC-SFOWT	6.01×10^6	1.47×10^7	3.78×10^6	1.77×10^6
Roll	TC-SFOWT	2.05×10^{10}	2.68×10^9	5.78×10^8	7.32×10^8
	FC-SFOWT	2.08×10^{10}	5.23×10^9	6.69×10^8	8.34×10^8
Pitch	TC-SFOWT	2.05×10^{10}	2.63×10^9	5.78×10^8	7.32×10^8
	FC-SFOWT	2.08×10^{10}	4.58×10^9	6.69×10^8	8.25×10^8

5.3. Dynamic Analysis of Towing System

5.3.1. Natural Frequencies

The natural frequencies of the heave, roll, and pitch motion for the two forms of SFOWT were studied by performing numerical decay tests in SIMO. The time series of free-decay can be obtained and plotted as shown in Figure 11, and the natural frequencies can be calculated based on the fast Fourier transform (FFT) method [28], as shown in Table 6.

Table 6. Natural frequencies in 3 DOFs of the SFOWTs.

DOFs		Frequency (Hz)
Heave	TC-SFOWT	0.070
	FC-SFOWT	0.056
Roll	TC-SFOWT	0.025
	TC-SFOWT	0.026
Pitch	FC-SFOWT	0.024
	FC-SFOWT	0.026

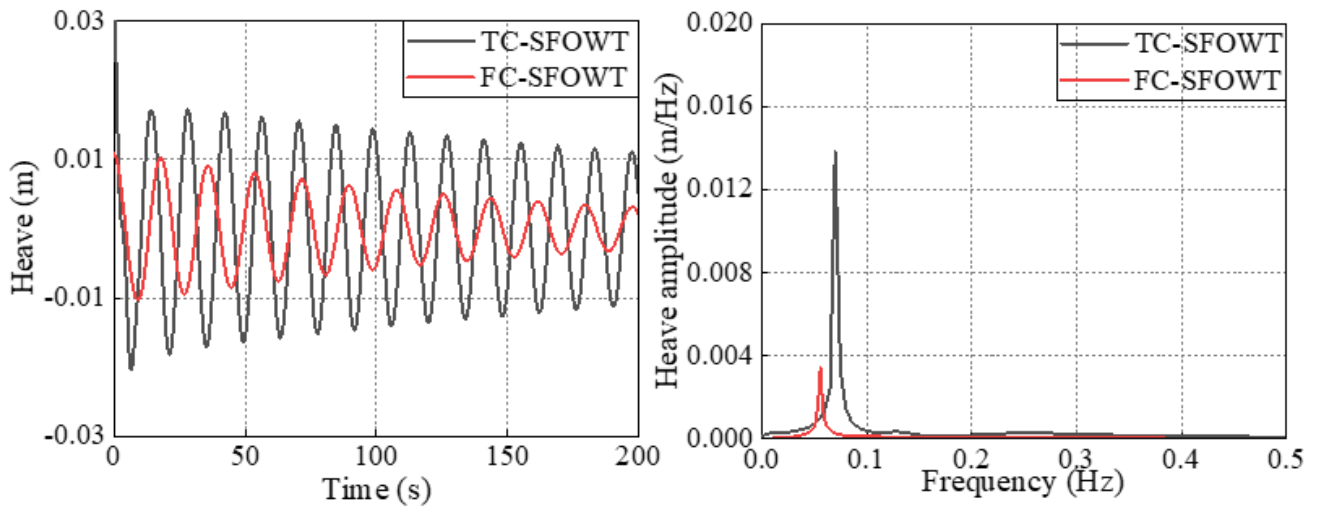
5.3.2. Influence of the Wave Height

Table 7 shows four wave conditions with different significant wave heights to study the influence of wave height on the integrated towing process. The water depth was 72 m, and the sea bottom was assumed to be flat. The JONSWAP wave spectrum was selected, and the simulation was performed for 3 h.

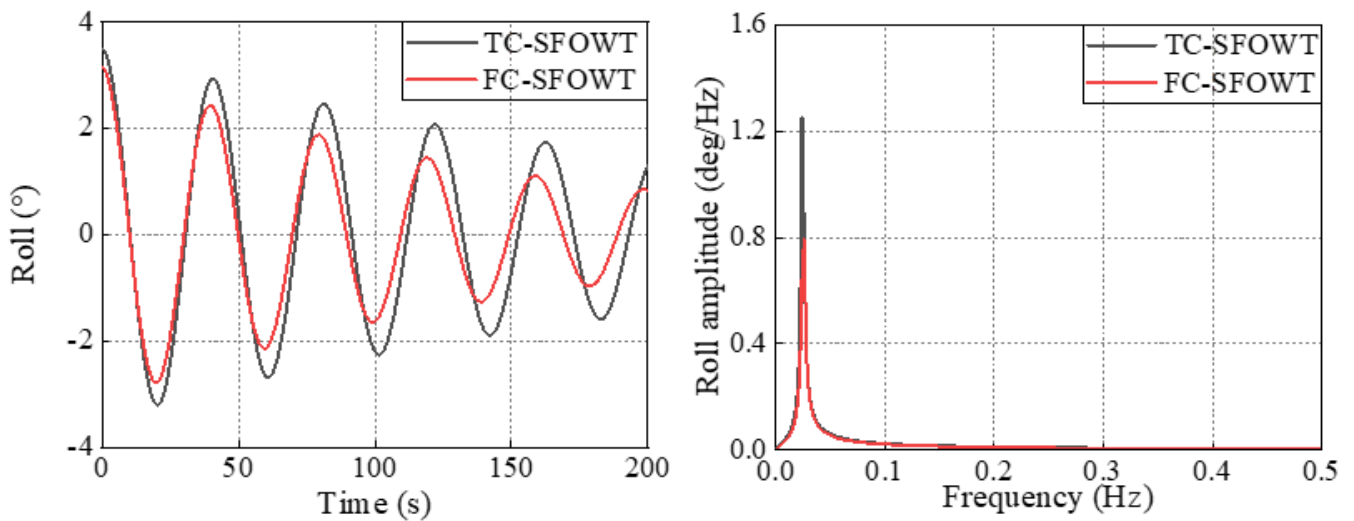
Table 7. Typical wave conditions under different wave heights.

Wave Conditions	C1	C2	C3	C4
Significant wave height (H_s)	2 m	3 m	4 m	5 m
Peak period (T_p)	8.9 s	8.9 s	8.9 s	8.9 s

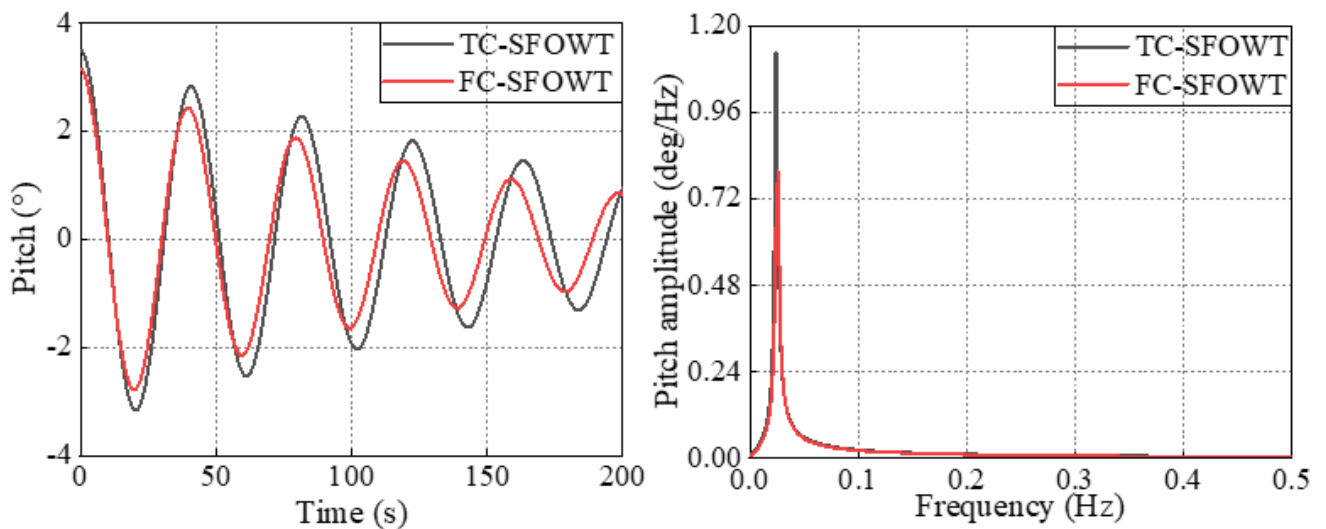
Figures 12 and 13 show the time series and statistics of heave, pitch, roll motion, and towing force of SFOWTs under different wave height conditions. It can be seen from the figures that the wave height has a significant influence on the responses of SFOWTs. When the significant wave height is 2 m, the maximum value of heave motion for TC-SFOWTs is 1.06 m, increasing by 43.4%, 99.1%, and 136.8%, respectively, when the significant wave heights are 3, 4, and 5 m. The maximum values of heave motion for FC-SFOWTs under different conditions are 0.86, 1.27, 1.71, and 2.25 m, respectively, and the maximum and minimum values of heave motion are lower than those of TC-SFOWTs under the same wave condition. The increase of wave height has a significant effect on the inclination of SFOWTs during the towing process. When the significant wave height is 5 m, the maximum value of pitch and roll motions of TC-SFOWTs are 2.14 and 1.38°, respectively, and they are 2.70 and 1.21° for FC-SFOWTs, respectively. The mean towing forces of TC-SFOWTs and FC-SFOWTs are 104.1 and 159.1 t, respectively, under C4. The pitch motion of the FC-SFOWT is larger, while the roll motion is smaller than those of the TC-SFOWT under the same wave condition. In addition, the mean towing force of the FC-SFOWT is larger than that of the TC-SFOWT under the same wave height condition.



(a)



(b)



(c)

Figure 11. Free-decay and frequency spectrum. (a) Free-decay in heave motion, (b) free-decay in roll motion, (c) free-decay in pitch motion.

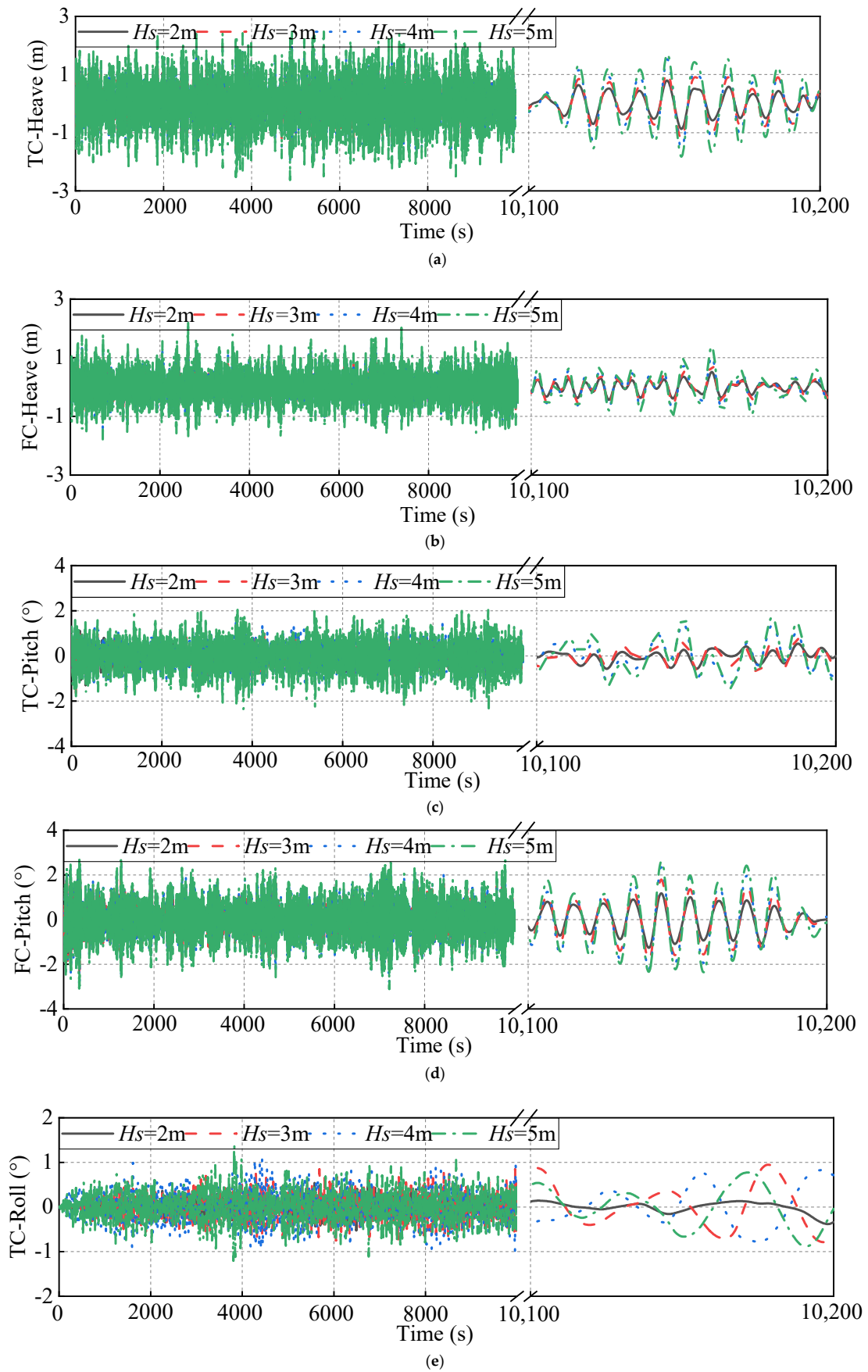


Figure 12. Cont.

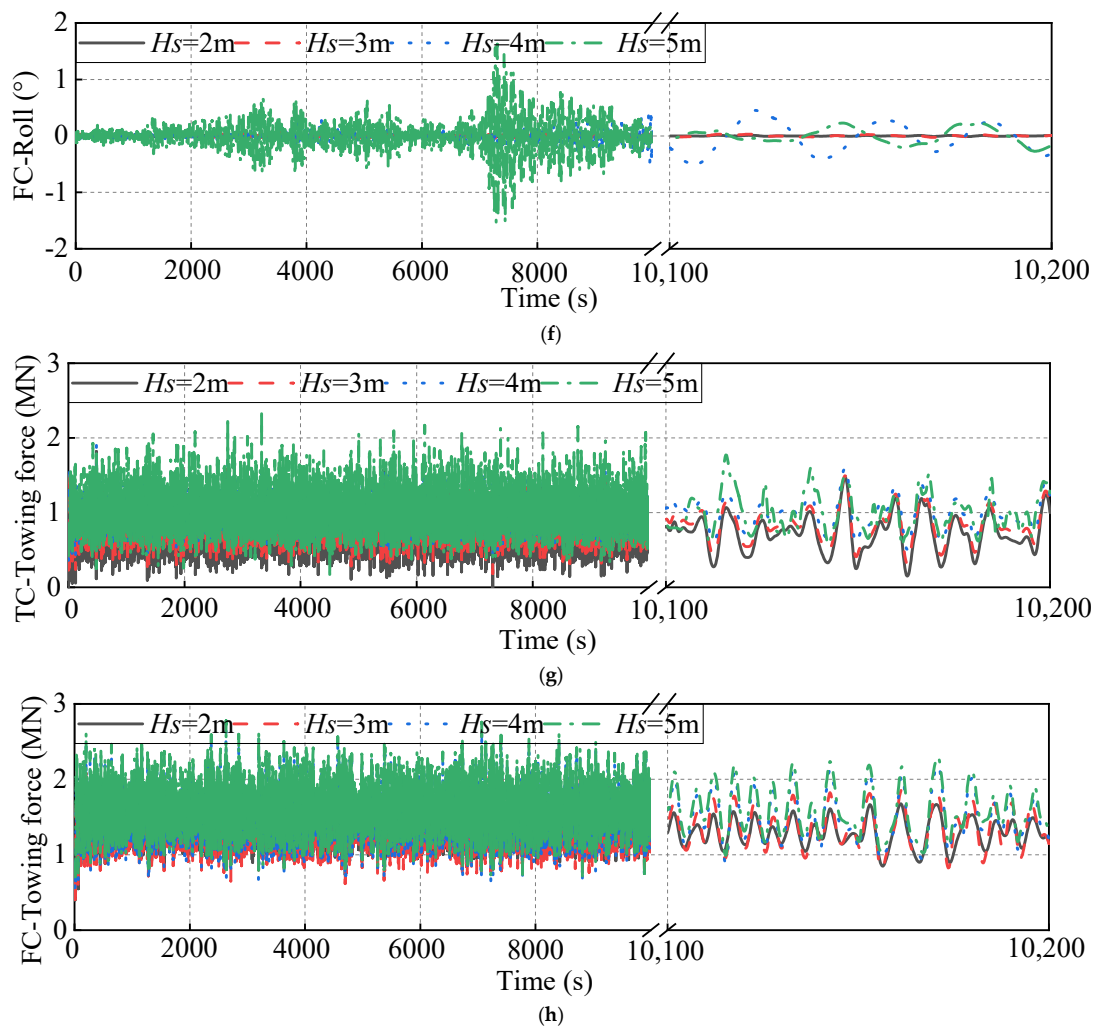


Figure 12. Time series of the SFOWT under different wave height conditions ($T_p = 8.9s$). (a) Heave motion of TC-SFOWT, (b) heave motion of FC-SFOWT, (c) pitch motion of TC-SFOWT, (d) pitch motion of FC-SFOWT, (e) roll motion of TC-SFOWT, (f) roll motion of FC-SFOWT, (g) towing force of TC-SFOWT, (h) towing force of FC-SFOWT.

Figure 14 shows the power spectra density (PSD) of the heave, pitch, and roll motion during the towing process at the different significant wave height conditions. Because the wave period for different conditions is the same, the frequencies corresponding to the heave, pitch, and roll peak of the SFOWTs are changeless under different conditions. The heave peak was more affected by significant wave height, as shown in Figure 14a, because the heave frequency of the SFOWTs was consistent with the wave frequency during the towing process. It can be seen from Figure 14c that the roll response of SFOWTs during the towing process was mainly caused by the resonance excited by wave-frequency loads. However, the main wave frequency range is 0.05~0.15 Hz, which avoids the roll natural frequency of SFOWTs (0.025 Hz for TC-SFOWT and 0.026 Hz for FC-SFOWT), so the frequency where the roll peak was appearing was less affected by the significant wave height changes.

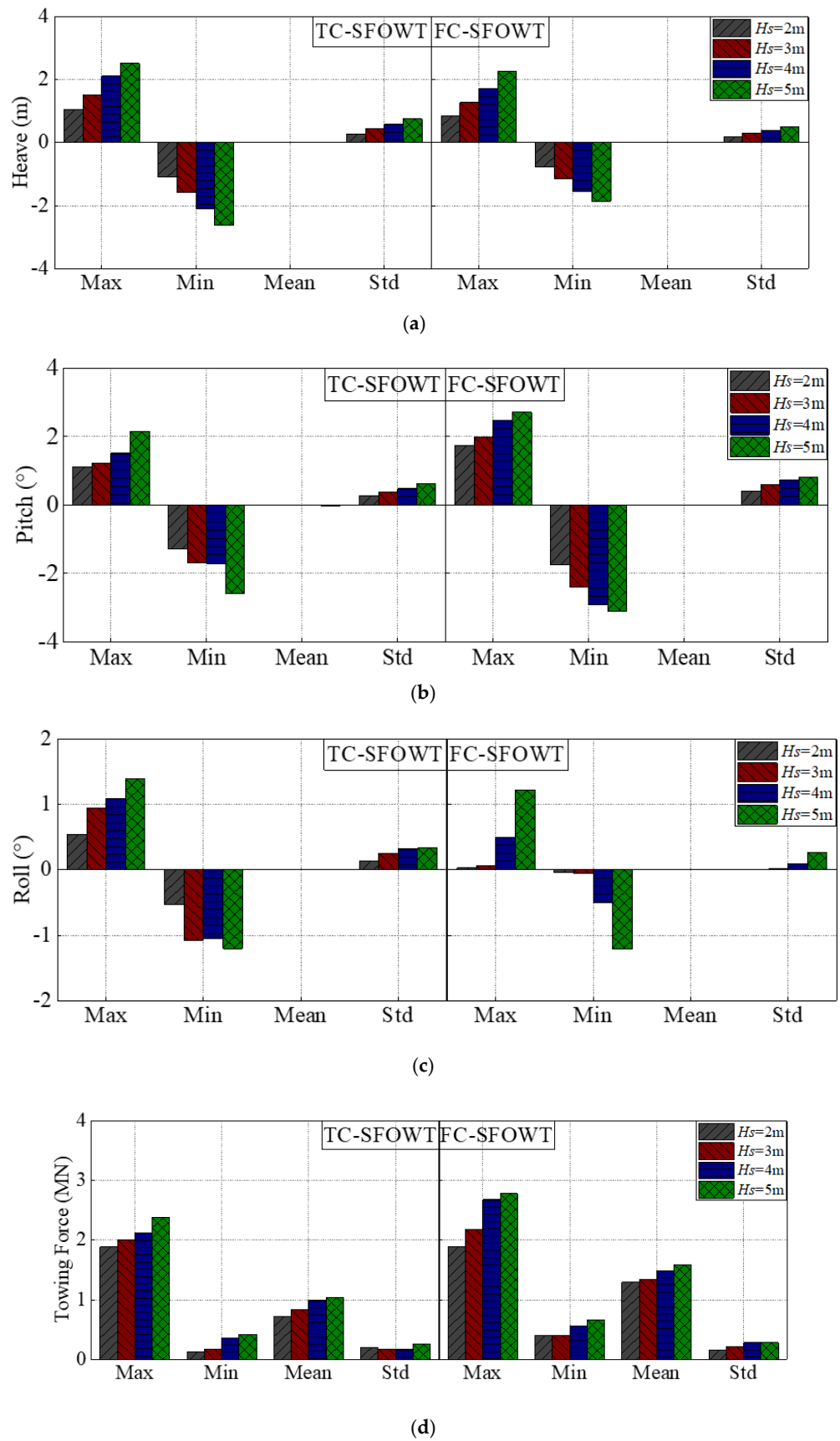


Figure 13. Statistics of the SFOWTs under different wave height conditions ($T_p = 8.9$). (a) Heave motion, (b) pitch motion, (c) roll motion, (d) towing force.

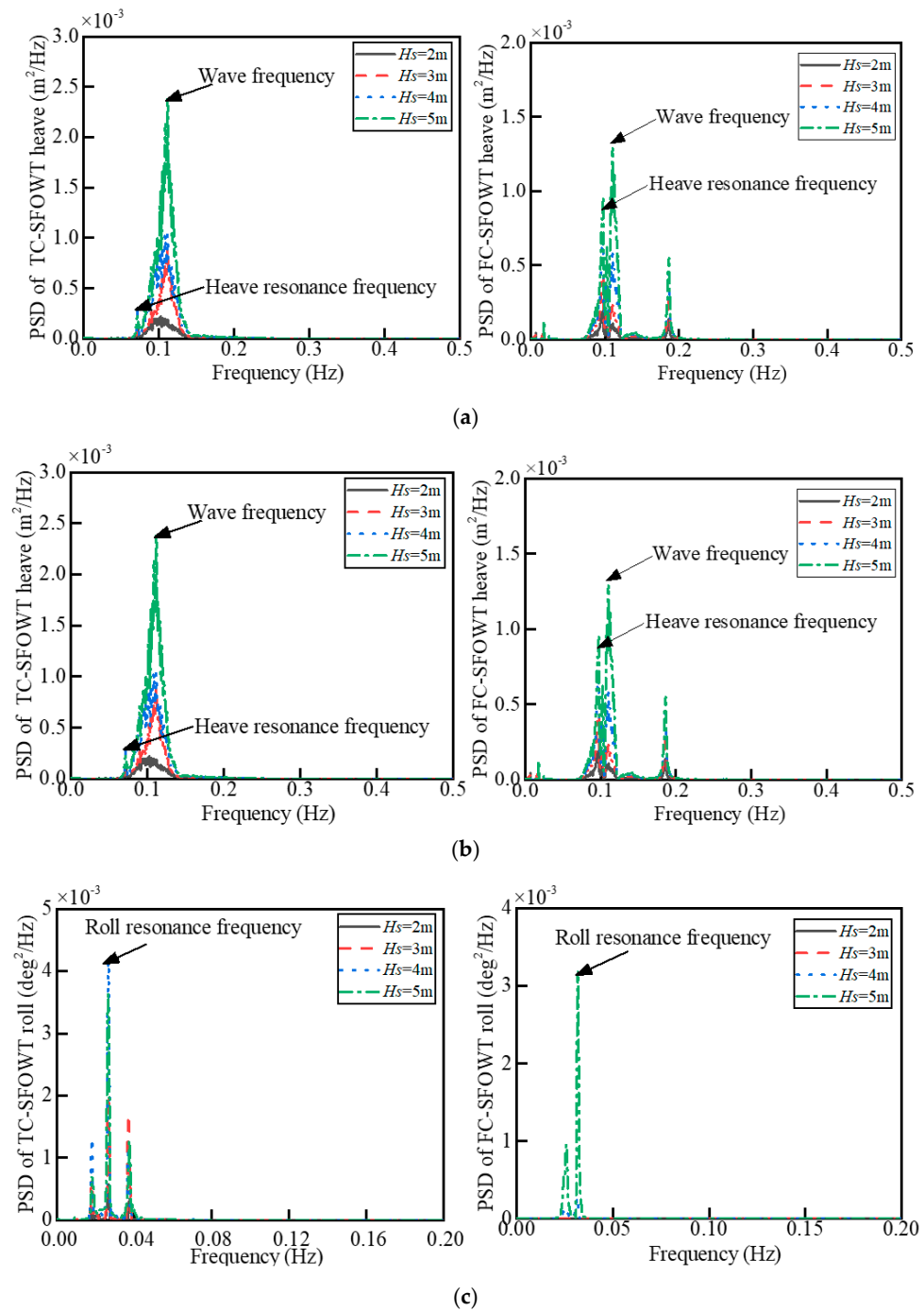


Figure 14. Power spectra of the SFOWT motion under different wave height conditions ($T_p = 8.9$ s). (a) Heave motion, (b) pitch motion, (c) roll motion.

5.3.3. Influence of the Wave Period

Table 8 shows four wave conditions with different wave periods to study the influence of the wave period on the towing process.

Table 8. Typical wave conditions under different wave periods.

Wave Conditions	C5	C6	C7	C8
Significant wave height (H_s)	5 m	5 m	5 m	5 m
Peak period (T_p)	8.9 s	11.6 s	13.4 s	15.2 s

Figures 15 and 16 are the time series and statistics of SFOWTs under different wave period conditions. The peak period has great influence on the heave motion of TC-SFOWTs. With the increase of the peak period, the maximum value of heave motion increases. When the peak period is 15.2 s, it is close to the heave natural period (14.3 s) of the TC-SFOWT, and the maximum value is 2.5 m, which increases by 62.6%, 10.2%, and 1.8% more than that of C5–C7, respectively. Peak period has little influence on the pitch motion of SFOWTs, and the pitch of FC-SFOWTs is larger than TC-SFOWTs under the same condition. When the peak period is 15.2 s, the mean towing forces of TC-SFOWTs and FC-SFOWTs are 138.1 and 180.3 t, which increase by 38.0% and 14.5% more than those under the C5, respectively. Under the same wave condition, a larger towing force is needed for FC-SFOWTs to obtain the same towing speed.

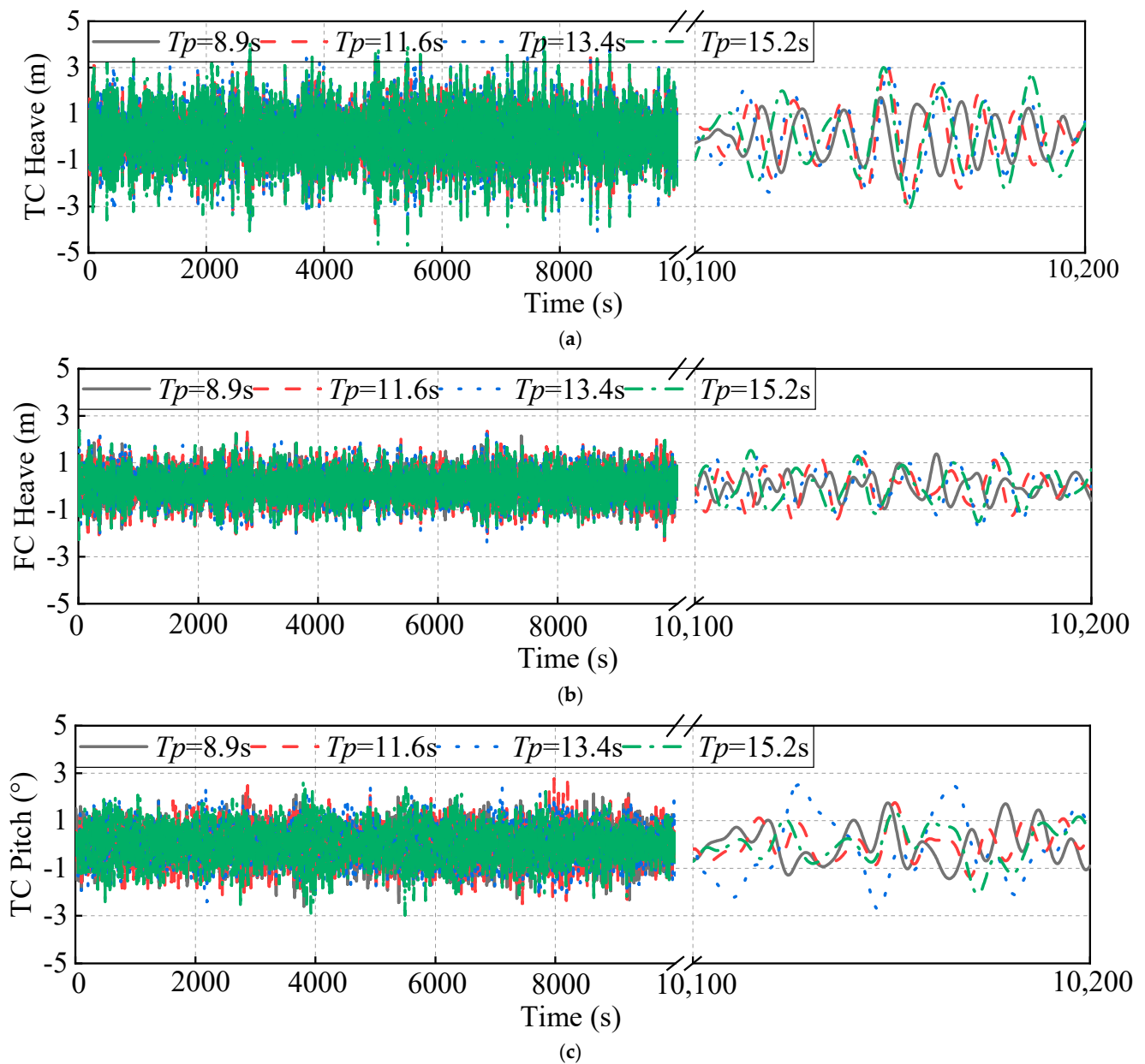


Figure 15. Cont.

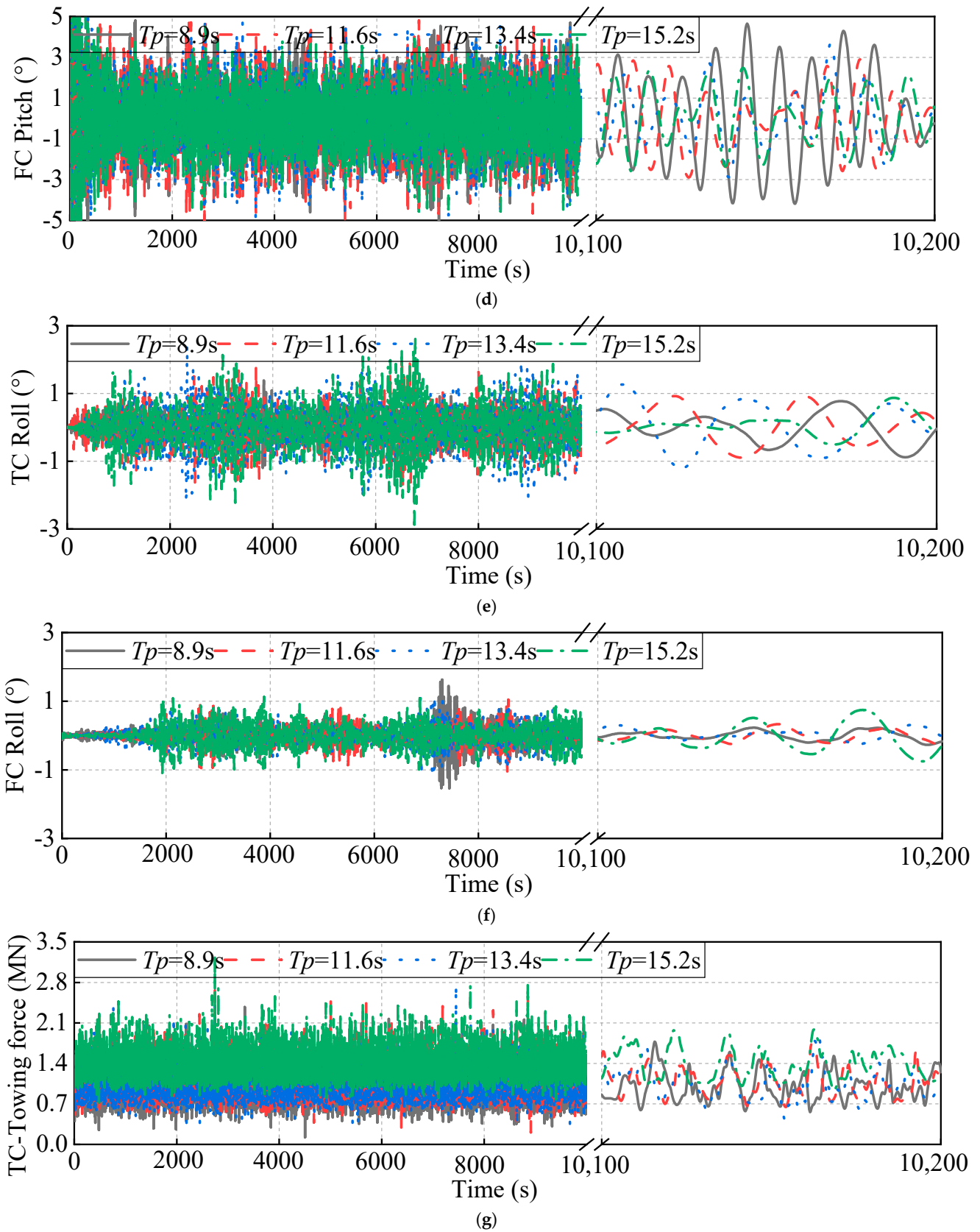


Figure 15. Cont.

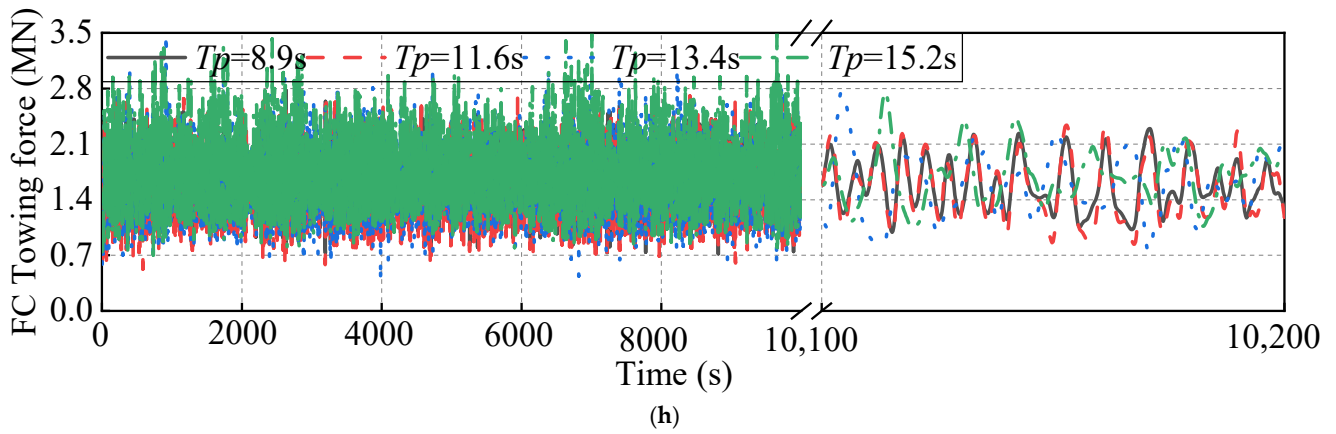


Figure 15. Time series of the SFOWTs under different wave period conditions ($H_s = 5$ m). (a) Heave motion of TC-SFOWT, (b) heave motion of FC-SFOWT, (c) pitch motion of TC-SFOWT, (d) pitch motion of FC-SFOWT, (e) roll motion of TC-SFOWT, (f) roll motion of FC-SFOWT, (g) towing force of TC-SFOWT, (h) towing force of FC-SFOWT.

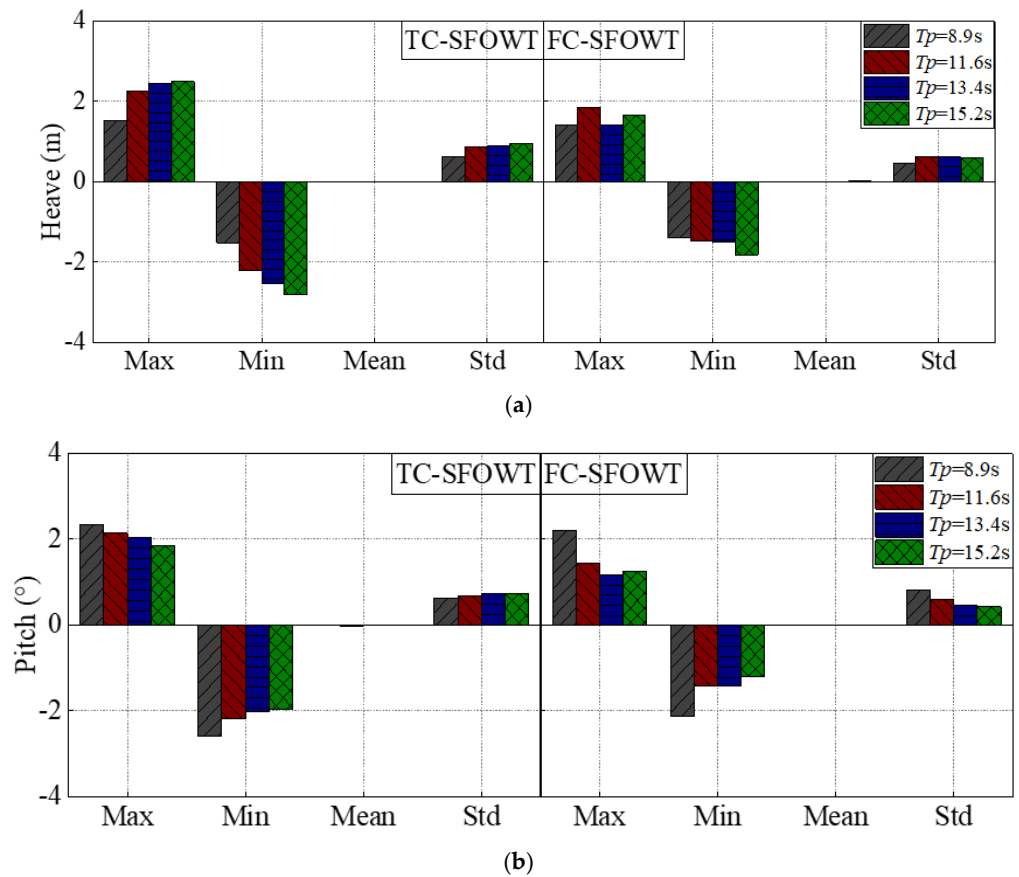


Figure 16. Cont.

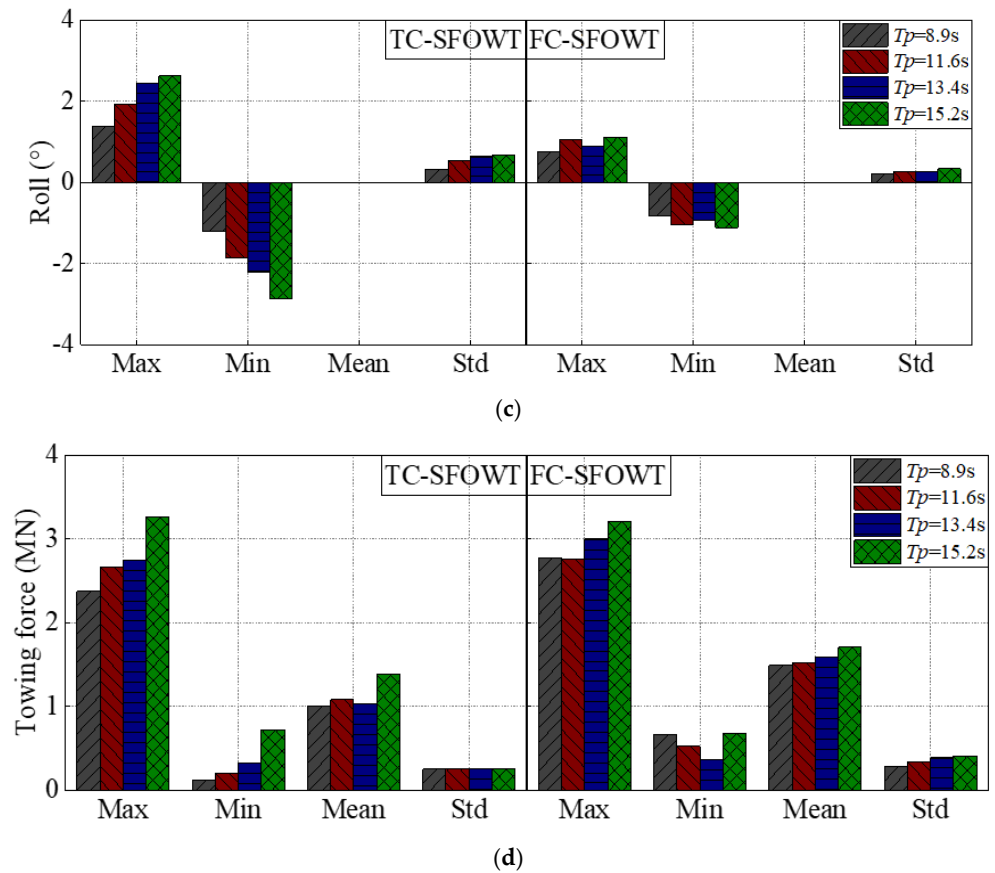


Figure 16. Statistics of the SFOWTs under different wave period conditions ($H_s = 5$ m). (a) Heave motion, (b) pitch motion, (c) roll motion, (d) towing force.

Figure 17 shows the power spectra density (PSD) of the heave, pitch, and roll motion during the towing process under different peak period conditions. The influence on the heave motion of SFOWTs is that the heave peak appears at the frequency corresponding to the peak period, but the value of the heave peak is less affected by the changes of the peak period. For pitch motion, with the increase of the peak period, the value of the peak which appears at the pitch resonance frequency increases, but the value of the other peak which appears at the frequency corresponding to the peak period changes little. Since the roll peak of SFOWTs appears at the resonance frequency excited by wave loads, the change of peak period will only affect the value of the roll peak, but has little influence on its occurrence frequency.

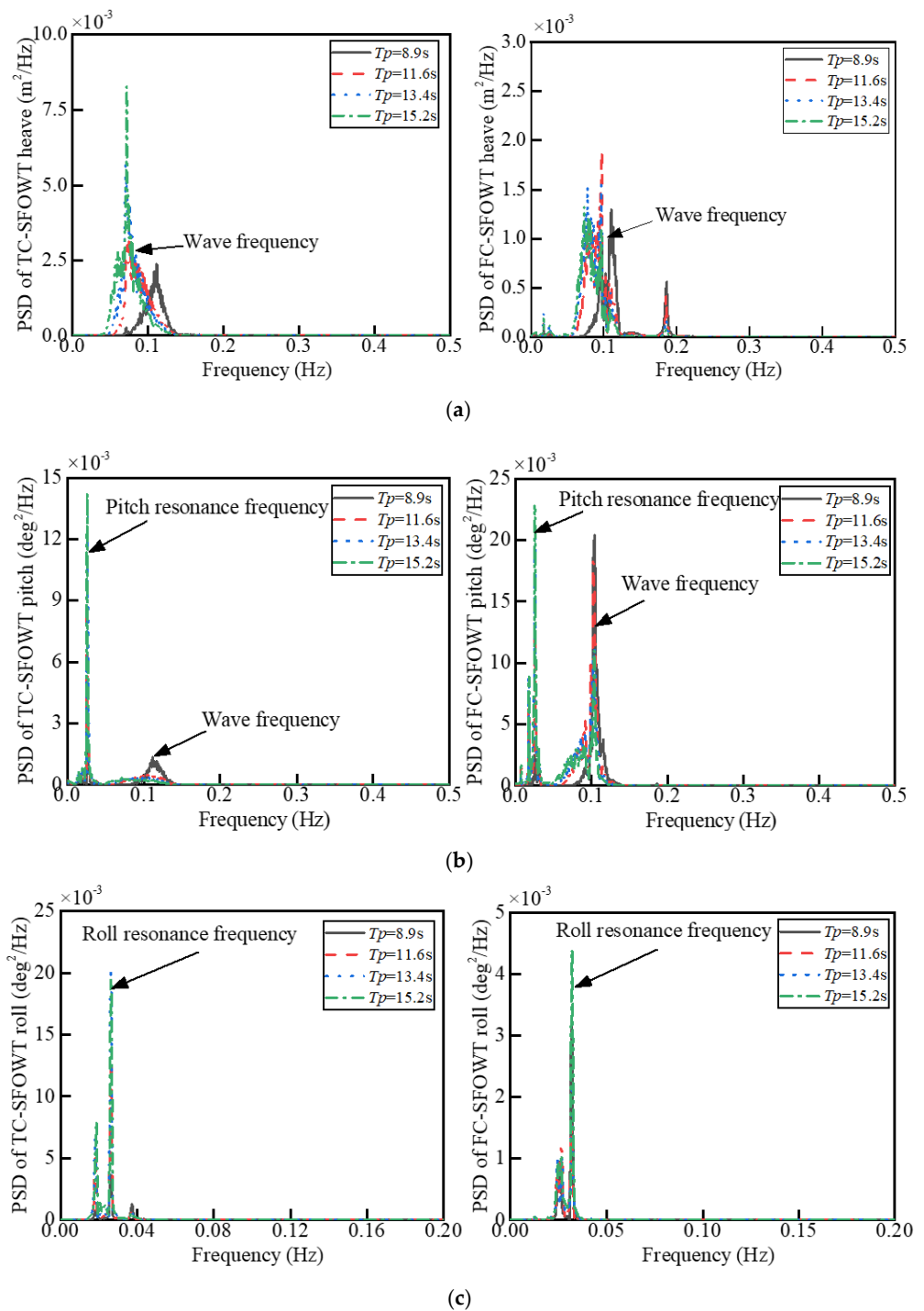


Figure 17. Power spectra of the SFWOT motion under different wave period conditions ($H_s = 5\text{ m}$). (a) Heave motion, (b) pitch motion, (c) roll motion.

6. Conclusions

In this paper, a comparative study of towing performance among the FC-SFWOTs and TC-SFWOTs under different wave conditions was performed. The effect of wave height and wave period in irregular wave conditions on the responses of heave, pitch, and roll motion and the towing force were discussed based on the potential flow theory considering the viscous damping.

RAOs in the heave, roll, and pitch motion were studied. When the wave period was greater than 32 s, the heave response of the two forms of SFWOT was less affected by the

wave period and the heave RAOs tended to be stable at the maximum value of 1 m/m. As for the RAOs in roll motion, they were similar in long-period wave conditions of the two forms of SFOWT, but the short-period wave had a great influence on the roll RAOs of FC-SFOWTs. In addition, the changes of RAOs in the pitch and roll motions of the two forms of SFOWT were similar.

The heave, pitch, and roll motion response and towing force of the two forms of SFOWT increase with the increase of significant wave height, and the heave motion was significantly affected by the change of wave height. When the significant wave height was 2 m, the maximum values of heave motion for TC-SFOWTs were 1.06, 1.52, 2.11, and 2.51 m, respectively; when the significant wave heights were 3, 4, and 5 m, they were 0.86, 1.27, 1.71, and 2.25 m, respectively, for FC-SFOWTs. The maximum roll and pitch motion amplitudes were 2.14 and 1.38°, respectively, for the TC-SFOWT, and 2.70 and 1.21°, respectively, for the FC-SFOWT when the significant wave height was less than 5 m, which is the maximum wave height for the allowable towing condition. Both the roll motion and the pitch motion are satisfied with the requirement that the roll and pitch are less than 5° during the towing process. The mean towing force of FC-SFOWT was 159.1 t, increasing by 52.8% compared with the TC-SFOWT, when the significant wave height was 5 m. The peak period mainly affected the frequency where the peak of motions appeared in power spectra. The heave peak appeared at the frequency corresponding to the peak period, but the value of the heave peak was less affected by the changes of the peak period. As for the roll motion, the change of the peak period only affected the value of the roll peak, but had little influence on its occurrence frequency in power spectra. Under the same wave condition, the FC-SFOWT showed relatively better performance in the platform motion, but the towing force was relatively larger compared with the TC-SFOWT.

In the next steps, the influence of more variables, such as the wind, current, the towing speed, and the layout of the mooring lines on the towing performance for two forms of SFOWT can be discussed. Furthermore, it is necessary to predict the towing performance of SFOWTs in damaged conditions.

Author Contributions: Conceptualization, C.L., P.Z. and H.D.; Methodology, C.L. and J.R.; Software, J.R. and C.L.; Validation, C.L., P.Z. and H.D.; Formal Analysis, J.R. and C.L.; Writing—Original Draft Preparation, J.R., C.L. and K.W.; Writing—Review and Editing, C.L., J.R., K.W.; Supervision, C.L., P.Z. and H.D.; Project Administration, C.L., H.D. and P.Z.; Funding Acquisition, C.L., H.D. and P.Z. All authors have read and agreed to the published version of the manuscript.

Funding: This research was funded by the Tianjin Municipal Natural Science Foundation (Grant No. 18JCYBJC22800); Special fund for promoting high-quality economic development of province in 2020 from Department of Natural Resources of Guangdong Province (Grant No. GDNRC [2020]015), and General Program of Natural Science Foundation of Guangdong Province, China (Grant No. 2021A1515011771).

Institutional Review Board Statement: Not applicable.

Informed Consent Statement: Not applicable.

Data Availability Statement: Not applicable.

Conflicts of Interest: The authors declare no conflict of interest.

References

1. Skaare, B.; Nielsen, F.G.; Hanson, T.D.; Yttervik, R.; Havmøller, O.; Rekdal, A. Analysis of measurements and simulations from the Hywind Demo floating wind turbine. *Wind Energy* **2015**, *18*, 1105–1122. [[CrossRef](#)]
2. Global Wind Energy Council (GWEC). *Global Wind Report 2021*; GWEC: Brussels, Belgium, 2021.
3. Guillaume, B.; Christian, B.; Christine, B.; Cecile, M.; Timothee, P.; Yann, P. Design and Performance of a TLP Type Floating Support Structure for a 6MW Offshore Wind Turbine. In Proceedings of the Offshore Technology Conference, Houston, TX, USA, 6–9 May 2019.
4. Blue H Engineering. Historical Development [N/OL]. Available online: <https://www.blueengineer-ing.com/historical-development.html> (accessed on 1 May 2021).

5. Adam, F.; Myland, T.; Dahlhaus, F.; Großmann, J. GICON®-TLP for Wind Turbines—the Path of Development. In Proceedings of the 1st International Conference on Renewable Energies Offshore (RENEW), Lisbon, Portugal, 24–26 November 2014; pp. 24–26.
6. Vita, L.; Ramachandran, G.K.V.; Krieger, A.; Kvittem, M.I.; Merino, D.; Cross-Whiter, J.; Ackers, B.B. Comparison of Numerical Models and Verification Against Experimental Data, Using pilaster TLP Concept. In *Proceedings of the International Conference on Offshore Mechanics and Arctic Engineering, St. John's, NL, Canada, 31 May–5 June 2015*; American Society of Mechanical Engineers: London, UK, 31 May 2015; p. V009T09A047.
7. European Wind Energy Association (EWEA). *The Economics of Wind Energy*; EWEA: Brussels, Belgium, 2015.
8. Strandhagen, A.; Schoenherr, K.E.; Kobayashi, F.M. The dynamic stability on course of towed ship. *SNAME* **1950**, *58*, 32–66.
9. Inoue, S.; Kakizaki, S.; Kasai, H.; Kubota, T.; Yamashita, Y. The course stability of towed boats. *Trans. West Jpn. Soc. Nav. Archit.* **1971**, *42*, 11–26.
10. Inoue, S.; Lim, S.T. The course stability of towed boats (continued). *Trans. West Jpn. Soc. Nav. Archit.* **1971**, *43*, 35–44.
11. Inoue, S.; Lim, S.T. The course stability of towed boats—When the mass of tow rope is continued. *Trans. West Jpn. Soc. Nav. Archit.* **1972**, *44*, 129–140.
12. Varyani, K. Course Stability Problem Formulation. In Proceedings of the 13th International Conference on Hydrodynamic in Ship Design (HYDRONAV 99), 2nd International Symposiums on Ship Manoeuvring (MANOEUVRING 99), Gdansk, Poland, 20–24 September 1999.
13. Collu, M.; Maggi, A.; Gualeni, P.; Rizzo, C.M.; Brennan, F. Stability requirements for floating offshore wind turbine (FOWT) during assembly and temporary phases: Overview and application. *Ocean Eng.* **2014**, *84*, 164–175. [[CrossRef](#)]
14. Hyland, T.; Adam, F.; Dahlhaus, F.; Großmann, J. Towing tests with the GICON®-TLP for wind turbines. In Proceedings of the 24th International Ocean and Polar Engineering Conference, Busan, Korea, 15–20 June 2014; pp. 283–287.
15. Ding, H.; Han, Y.; Zhang, P. Dynamic analysis of a new type of floating platform for offshore wind turbine. In Proceedings of the 26th International Ocean and Polar Engineering Conference, Rhodes, Greece, 26 June–2 July 2016.
16. Le, C.; Li, Y.; Ding, H. Study on the coupled dynamic responses of a submerged floating wind turbine under different mooring conditions. *Energies* **2019**, *12*, 418. [[CrossRef](#)]
17. Le, C.; Zhang, J.; Ding, H.; Zhang, P.; Wang, G. Preliminary Design of a Submerged Support Structure for Floating Wind Turbines. *J. Ocean Univ. China* **2020**, *19*, 1265–1282. [[CrossRef](#)]
18. Ding, H.; Han, Y.; Zhang, P.; Le, C. Dynamic Analysis of a Floating Wind Turbine in Wet Tows Based on Multibody Dynamics. *J. Renew. Sustain. Energy* **2017**, *9*, 033301. [[CrossRef](#)]
19. Han, Y.; Le, C.; Ding, H.; Cheng, Z.; Zhang, P. Stability and dynamic response analysis of a submerged tension leg platform for offshore wind turbines. *Ocean Eng.* **2017**, *129*, 68–82. [[CrossRef](#)]
20. Gerwick, C. *Construction of Marine and Offshore Structures*; CRC Press: Boca Raton, FL, USA, 2002.
21. Bak, C.; Zahle, F.; Bitsche, R.; Kim, T.; Yde, A.; Henriksen L., C.; Natajaran, A.; Hansen M., H. *Description of the DTU 10 MW Reference Wind Turbine*; Technical Report; Technical University of Denmark Wind Energy: Roskilde, Denmark, 2013.
22. DNV. SESAM User Manual GenIE v6.4. Concept Design and Analysis of Offshore Structures. Det Norsk Veritas. 2013. Available online: https://www.dnv.com/services/conceptual-modelling-of-offshore-and-maritime-structures-genie-89128?gclid=EAIAIQobChMIsc7AzaiC8QIVwRwrCh2QbQ6WEAAAYAiAAAEgJSUfD_BwE&gclidsrc=aw.ds (accessed on 4 June 2021).
23. DNV. SESAM User Manual HydroD v4.7. Wave Load & Stability Analysis of Fixed and Floating Structures. Det Norsk Veritas. 2014. Available online: <https://www.dnv.com/services/hydrodynamic-analysis-and-stability-analysis-software-hydrod-14492> (accessed on 4 June 2021).
24. DNV. *SIMO User Manual Version 4.0 rev 0*; Norwegian Marine Technology Research Institute, Marintek: Trondheim, Norway, 2012.
25. DNV. *SESAM User Manual WASIM. Wave Loads on Vessels with Forward Speed*; Marintek: Trondheim, Norway, 2006.
26. DNV. *DNV-RP-C205 Environmental Conditions and Environmental Loads*; Det Norske Veritas: Oslo, Norway, 2010.
27. Roddier, D.; Peiffer, A.; Aubault, A.; Weinstein, J. A generic 5MW WindFloat for numerical tool validation & comparison against a generic Spar. In Proceedings of the ASME 2011 30th International Conference on Ocean, Offshore and Arctic Engineering, Rotterdam, The Netherlands, 19–24 June 2011.
28. Cooley, J.W.; Lewis, P.A.; Welch, P.D. The fast Fourier transform and its applications. *IEEE Trans. Educ.* **1969**, *12*, 27–34. [[CrossRef](#)]